Dielectric spectroscopy of hydrogen treated hexagonal boron nitride ceramics

Journal:	*ACS Applied Electronic Materials*
Manuscript ID	el-2019-00767y.R2
Manuscript Type:	Article
Date Submitted by the Author:	04-Mar-2020
Complete List of Authors:	Cuenca, Jerome; Cardiff University School of Physics and Astronomy Mandal, Soumen; Cardiff University, Morgan, David; Cardiff University, Cardiff Catalysis Institute Snowball, Malcolm; Ultra Biotecs Ltd Porch, Adrian ; Cardiff University Cardiff School of Engineering Williams, Oliver; Cardiff University, School of Physics and Astronomy

Dielectric spectroscopy of hydrogen treated hexagonal boron nitride ceramics

Jerome A. Cuenca,*,† Soumen Mandal,† David J. Morgan,‡ Malcolm Snowball,¶ Adrian Porch,§ and Oliver A. Williams†

†*Cardiff School of Physics and Astronomy, Cardiff, CF24 3AA, UK*

‡*Cardiff Catalysis Institute, School of Chemistry, Cardiff, CF10 3AT , UK*

¶*Ultra Biotecs Limited, Derby, DE24 9FU, UK*

§*Cardiff School of Engineering, Cardiff, Wales, CF24 3AA, UK*

E-mail: cuencaj@cardiff.ac.uk

Abstract

Hexagonal boron nitride (h-BN) is a critical material for 2D electronic devices and has attracted considerable attention owing to its structural similarity to graphene. However, it is a dielectric and modifying its electrical properties is a challenge. Hydrogenation has been calculated as a potential method, although is rarely experimentally measured. Here, dielectric spectroscopy of hot-pressed h-BN after various hydrogen treatments has been investigated. Untreated h-BN showed a frequency independent dielectric constant (4.2 ± 0.2) and an immeasurably low dielectric loss factor, demonstrating the ideal dielectric nature of h-BN across the 10^3 to 10^{10} Hz range. However, hydrogen plasma (H^+) treatment in a microwave chemical vapour deposition (CVD) reactor amplified the complex permittivity dramatically, introducing Havriliak-Negami (HN) type dispersion ($\varepsilon_s \approx 20 \pm 2$, $\varepsilon_\infty \approx 4.2 \pm 0.2$) and a percolating long range conductivity (~ 0.32 mS/m). Annealing in molecular hydrogen (H_2) at similar CVD temperatures showed minimal impact, implying that H_2 diffusion is not the cause. Oxygen plasma treatment, however, removes the percolating conductivity but the Debye mechanism remains. This leads to the conclusion that the electrical conductivity of h-BN ceramics can be modified through hydrogenation, using atomic hydrogen. The potential as a tunable wide-band gap semiconductor is highlighted however for insulating dielectric substrate applications, microwave CVD may destroy these desirable properties.

Keywords

hexagonal boron nitride, dielectric spectroscopy, complex permittivity, hydrogenation, microwave hydrogen plasma

1 Introduction

The dielectric properties of hexagonal boron nitride (h-BN) have received recent interest owing to its two-dimensional (2D) structural similarity to graphene, albeit electrically insulating. Since graphene is incredibly sensitive to the environment, dielectric encapsulation using h-BN is a possible stabilisation method.[1–3] h-BN has a small lattice mismatch with graphene of approximately 1.5 to 1.7%,[4,5] a high band gap of 5.97 eV,[4] high dielectric strength[6] and a low dielectric constant (ranging from 2 to 5).[7,8] There are also contrasting dielectric applications of h-BN, including microwave absorbing composites using h-BN as an insulating inclusion, as well as potential biomedical applications.[9–12] As a dielectric substrate for graphene, h-BN is commonly produced using thin film sputtering or chemical vapour deposition (CVD). The resultant material may also include unwanted BN phases including amorphous and turbostratic boron nitride (a-BN and t-BN). Recent progress has been made through sputtering onto nanocrystalline diamond substrates, with a lower density of a-BN and t-BN, although at slow deposition rates of hundreds of nanometres per hour.[13] The hot-pressed method can produce thick h-BN ceramics using boric acid binders, with pores leading to an increased hygroscopicity. From an electronic device perspective, thicker dielectrics of h-BN are favourable to contain stray electromagnetic fields.

Graphene deposition using CVD involves exposing the substrate to a carrier gas at high temperatures (>800 °C). Successful deposition has been demonstrated using microwave plasma CVD in hydrogen (H_2) on Cu substrates.[14,15] h-BN substrates can survive these high temperatures (stability up towards ∼1000 °C).[16] It would be assumed that the favourable low dielectric constant of the h-BN is unchanged, however, like graphene, sp^2 bonding is

prone to etching. Reactive H^+ ions are known to etch sp^2 in BN,[17] partially transform sp^2 into sp^3 through hydrogen termination of dangling bonds[18] and diffuse through and distort h-BN layers.[19] A change in the polarisability is expected, especially with hydrogenation, though this hypothesis is rarely tested. Also, the conventional tube furnace CVD methods, where graphene is deposited on h-BN in H_2 (>800 °C), may also affect the dielectric properties.[20–22]

Dielectric spectroscopy of h-BN is an important research area for low dielectric constant graphene substrates and while there is much in the literature on its *calculation*, experimental measurements are uncommon, let alone studies of hydrogenation. Notable works in the radio frequency (RF) domain by Kim et al. demonstrate the favourably low dielectric constant,[7] while Shi et al. show layer stacking effects of BN.[23] Previous dielectric measurements have been conducted in the RF or optical range, though rarely at microwave frequencies.[24]

This work shows the effect of atomic and molecular hydrogen treatment (plasma and annealing) on the broadband (10^3 to 10^{10} Hz) dielectric properties of h-BN, achieved using well-established non-destructive dielectric spectroscopy methods, including parallel plate capacitor (PPC), broadband coaxial probe (BCP) and microwave cavity perturbation (MCP).[25,26]

2 Theory

2.1 Complex permittivity

The complex permittivity is defined as the ability of a material to polarise in an electric field with the imaginary part associated with the time-harmonic polarisation loss:

$$\varepsilon_{\mathrm{r}}(\omega) = \varepsilon'_{\mathrm{r}}(\omega) - j\varepsilon''_{\mathrm{r}}(\omega) \tag{1}$$

where $\varepsilon'_{\mathrm{r}}(\omega)$ is the frequency dependent dielectric constant, $\varepsilon''_{\mathrm{r}}(\omega)$ is the dielectric loss factor, ω is angular frequency in rad/s or $2\pi f$ and f is frequency in Hz. Dielectric polari-

sation mechanisms in solids arise from free charge conductivity (Drude DC model), space charge polarisation in inhomogeneous conducting mixtures or dipolar relaxation (Drude AC or Debye/Havriliak-Negami models) and bound electronic polarisation (Lorentz model).[27] In the case of non-polar materials, dipolar relaxation is non-existent and so too are Lorentz based frequency dependent contributions from electronic relaxation when measuring at much lower than terahertz frequencies. For percolating free charge conductivity or long range conductivity, the dielectric loss factor follows:[28,29]

$$\varepsilon''_{\mathrm{r,\ Drude}}(f) \approx \frac{\sigma}{\omega\varepsilon_0} \tag{2}$$

where ε_0 is the permittivity of free space and σ is the free charge conductivity in S/m. A characteristic ω^{-1} dependence in the dielectric loss implies this mechanism. For space charge polarisation, both real and imaginary parts are modelled by Debye/Havriliak-Negami type relaxations:[27]

$$\varepsilon_{\mathrm{r,\ HN}} \approx \varepsilon_\infty + \left(\frac{\varepsilon_{\mathrm{s}} - \varepsilon_\infty}{[1 + (j\omega\tau)^\alpha]^\beta}\right) \tag{3}$$

where ε_{s} and ε_∞ are the low and high frequency dielectric constants, respectively, τ is the time constant of the hopping process and α and β are fitting exponents as empirical values rarely follow the ideal Debye model (where $\alpha = \beta = 1$). The result is a decrease in the real part and a loss peak at the relaxation frequency of $1/\tau$.

3 Experimental

The complex permittivity of most materials can be measured, broadly speaking, with two approaches: broadband transmission/reflection and resonant techniques, whereby the former allows the observation of dispersion from frequency dependent polarisation mechanisms while the latter methods offer high narrowband sensitivity.

3.1 Parallel plate method (PPC)

The parallel plate method is the simplest non-resonant approach to obtaining the complex permittivity, whereby the material is contacted using two metallic electrodes and impedance is measured, diagram shown in Figure 1. The complex permittivity is related through:[30]

$$C - j\frac{G}{\omega} = k_{\mathrm{eff}}\varepsilon_{\mathrm{r}}(\omega) \tag{4}$$

where C is the capacitance, G is the conductance, k_{eff} is a geometrical constant found from an air-measurement or of a known calibration sample. The first term of (4) can be obtained by measuring the fixture in free space. The sample must cover the entirety of the electrode, whereby the out-of-plane dielectric value is measured for flat samples.

3.2 Broadband coaxial probe (BCP)

The open ended coaxial probe is a reflection based method which uses a similar capacitance perturbing approach in that a coaxial cable is terminated into free space or a dielectric sample. The radial transverse electromagnetic fields which exist within the cable are suddenly interrupted by a free space section, giving rise to a predominantly parallel field with some perpendicular fields into the sample, diagram shown in Figure 1. Assuming that the sample occupies infinite space at the end of the probe, the complex permittivity can be obtained using the reflection coefficient. This assumption is fulfilled by having a sample several hundreds of microns thick for a millimetre small coaxial aperture. The impedance has been measured here through scattering parameters and the extraction of complex permittivity is approximated as follows:[25]

$$\varepsilon_{\mathrm{r}}(\omega) \approx \frac{1}{j\omega\varepsilon_0 C_0 Z_0}\left(\frac{1-\Gamma_{\mathrm{L}}/\Gamma_{\mathrm{a}}}{1+\Gamma_{\mathrm{L}}/\Gamma_{\mathrm{a}}}\right) + 1 \tag{5}$$

where Γ_L and Γ_a are the air and sample terminated complex reflection coefficients, respectively, Z_0 is the characteristic impedance taken as 50 Ω and C_0 is the probe capacitance which may be obtained by measuring a material of known dielectric constant. In this study, we have calibrated the BCP to a polytetrafluoroethylene (PTFE) standard.

3.3 Microwave cavity perturbation (MCP)

The microwave cavity perturbation method is a resonant technique whereby the sample is placed within the electric (E) or magnetic (H) fields of a microwave cavity resonator and the presence of the sample within the field alters the resonant frequency of the system, diagram shown in Figure 1. Differences in the unperturbed and perturbed response are attributed to the dielectric or magnetic properties, depending on the volume perturbation within the E or H field as given by the following:

$$-\frac{\Delta\omega}{\omega_0} \approx \frac{\varepsilon_r(\omega) - 1}{1 + N\left[\varepsilon_r(\omega) - 1\right]} \frac{V_s}{V_m} \tag{6}$$

where $\Delta\omega/\omega_0$ is the fractional change in complex resonance caused by a sample perturbation, V_s and V_m denote the sample volume and mode volume of the cavity, respectively and N is the geometric sample depolarising factor which is positive and less than or equal to unity.[26] For low permittivity samples placed in minimal depolarising geometry $N \approx 0$. In other cases, N may be obtained analytically, through finite element modelling, or through measurement of a known sample.[26,31]

4 Experimental Method

The samples used were commercially available hot-pressed h-BN ceramics used in previous studies.[32] The as received h-BN substrates have dimensions of $\sim 0.5 \times 10 \times 10$ mm. Hydrogen plasma treatment of the as received h-BN was carried out using a Seki Technotron AX6500 microwave CVD reactor (4 kW at 50 Torr, 500 sccm of H_2 for 1 hour at $\sim$ 800°C). The

substrate temperature was monitored using a Williamson dual wavelength pyrometer. After the H-plasma treated sample was measured, attempts to remove the hydrogenation through oxygen termination was achieved at room temperature using an RF oxygen plasma in an evacuated PE-25 Plasma Etch chamber (120 W, 30 sccm of O_2 for 1 minute). The annealed samples were treated using a furnace at $\sim$ 800 °C in vacuum or hydrogen ambient (100 sccm of H_2 at 7.5 Torr for 1 hour). Samples were also dipped in deionised water before annealing to encourage hydrogen uptake.

Material characterisation was carried out using Raman and x-ray photoelectron spectroscopy (XPS). Raman spectroscopy was conducted using a Renishaw inVia Reflex spectrometer with a green laser (λ = 514 nm, $\times$20 objective). Spectra was obtained from 3 separate regions on the sample surface and have been corrected by subtracting a background signal, fitted to a fourth order polynomial. XPS was conducted using a Thermo scientific K-Alpha system utilising a micro focused monochromatic Al Kα X-ray source operating at 72 W (6 mA x 12 kV). Survey scans were performed with coarse step energies of 1eV, and high resolution scans were performed with fine steps of 0.1 eV. Data was analysed using CasaXPS (v2.3.23) after removal of Shirley type background, using Scofiled sensitivity factors and an electron energy dependence of 0.6.

Dielectric measurements have been carried out from 1 kHz to 10 GHz. The PPC method has been conducted from 1 kHz to 1 MHz (Keysight E4990A impedance analyser and 16451B). For moderately conductive samples, electrode polarisation (EP) introduces an additional inverse power law artefact in PPC ($\propto f^{-\gamma}$).[33] This has been accounted for by assuming a static low frequency dielectric constant and extrapolating the BCP $\varepsilon'_{\mathrm{r}}$ value, revealing the long range conductivity component. The BCP method has been conducted from 10 MHz to 10 GHz (Keysight N5232A vector network analyser) with an estimated penetration depth of <0.2 mm.[25,34] MCP has been conducted with an Al rectangular cavity at 2.5, 4.6 and 5.5 GHz.[26] An additional WG14 waveguide cavity was used at 4.5, 5.6, 7.4 and 9.6 GHz to corroborate the Al cavity. For the unperturbed response, an acetate sheet was used to suspend

the sample in the centre of the cavity. Prior to sample measurement, a $1.5 \times 10 \times 10$ mm piece of PTFE was used as a calibration standard. The well-known non-dispersive dielectric nature of PTFE allowed the different methods to be lined up across the frequency range with the PPC value as reference. Multi-meter measurements were also obtained using probe contacting only. Metal contacts or devices were not deposited in order to preserve the surface integrity and to decouple any additional effects associated with the deposited electrodes. This means that all dielectric measurements are obtained at lower power, however, the advantages of using the PPC, BCP and MCP fixtures are that surface measurements can be made electronic properties without any additional electrode fabrication steps or significant surface damage.

5 Results

5.1 Complex permittivity

The measured complex permittivity of the PTFE, as received h-BN, plasma treated h-BN and annealed h-BN samples are given in Figures 2 and 3 and Tables 1 and 2. The PTFE standard gave a nominal value of 2.05 across the low kilohertz to megahertz frequency range. Since PTFE is assumed non-dispersive, this value is extrapolated to higher frequencies, allowing the PPC, BCP and MCP methods to be compared for the h-BN samples. It is also shown that there are considerable variations from 1 to 10 kHz which are systematic errors associated with the sensitivity of the measurement. From Table 2 the WG14 MCP measurements showed much higher losses with increasing frequency, particularly at 9.6 GHz. Since it is well-known that PTFE has negligible loss at gigahertz frequencies, the additional loss is likely a systematic error associated with the strong coupling to the resonator.

The as received h-BN gave a dielectric constant of 4.3 ± 0.1 in the kilohertz to megahertz range, in close agreement with the analytically calculated out-of-plane value.[35] Even though h-BN is 2D, the material is a compressed ceramic and so an anisotropic value was not

obtained, rather an averaged isotropic value. With increasing frequency, there was minimal change with a value of 4.2±0.2 obtained using the BCP method. In the gigahertz range, MCP corroborated the BCP values as shown in Table 1. As with the PTFE sample, the dielectric loss was immeasurable in the megahertz to gigahertz range, with the same artefact of the slight increase at 9.6 GHz. The negligible loss and low dielectric constant demonstrates the favourable insulating dielectric properties of h-BN.

After H-plasma treatment of the as received samples, the complex permittivity increased dramatically, with dispersive features. Starting with the MCP values at gigahertz frequencies, the dielectric constant increased from the untreated sample to 4.726 ± 0.006 at 2.5 GHz though remained at a similar value to the untreated of 4.101 ± 0.001 at 9.6 GHz. The dielectric loss, however, increased substantially from immeasurable to 1.48 ± 0.01 at 2.5 GHz and decreasing to 0.38 ± 0.01 at 9.6 GHz, characteristic of a relaxation process occurring at lower megahertz frequencies. The BCP data confirmed this relaxation mechanism, with an approximate Havriliak-Negami (HN) model ($\varepsilon_s = 20$, $\varepsilon_\infty = 4.2$, $\tau^{-1} = 150$ MHz, $\alpha = 0.9$ and $\beta = 1$). Finally, towards lower frequencies, the conductivity was large enough to induce EP in the PPC method. The corrected data, extrapolated from the BCP dielectric constant, revealed a percolating free charge conduction mechanism of approximately 0.32 mS/m. This value was corroborated with contacting multi-meter measurements of 0.1 to 0.5 mS/m. All other samples could not be measured due to their high resistivity.

When the as received h-BN samples were exposed to similar elevated temperatures in a H_2 atmosphere, minimal change in the complex permittivity was observed. Figure 3 shows that there was a small decrease in the overall dielectric constant and a very small increase in the low frequency loss. Similar values were obtained for vacuum annealed samples while wet annealing to encourage H_2 uptake also gave minimal change. This result demonstrates that exposing h-BN to H_2 at elevated temperatures has minimal impact to the electrical properties.

After exposing the H-Plasma treated sample to an RF O-plasma the dispersive features

change. Starting with the MCP values, the dielectric constant follows a similar trend to the H-Plasma sample, with slightly reduced values of 4.428 ± 0.006 at 2.5 GHz, decreasing to 3.892 ± 0.006 at 9.6 GHz, with measurements at intermediate frequencies following a similar trend. The lower values imply that the megahertz relaxation frequency has decreased. This is corroborated in the BCP measurement ($\tau^{-1} = 60$ MHz, $\alpha = 0.9$). At lower frequencies, however, the percolating conduction is non-existent. Consequently, no EP correction was needed at all on the sample. The static dielectric constant has remained similar to the H-plasma treated sample ($\varepsilon_s = 20$), however, a discrepancy in the HN relaxation behaviour is noticed between the PPC and BCP methods. The reason for this is due to the measurement technique, attributed to the different E field orientations and effective probing area; PPC measures perpendicular to the sample plane while BCP measures predominantly parallel as is shown in Fig. 1. Assuming that both measurements relax to the same ε_∞ value, the PPC relaxation occurs at a much lower frequency with a broader characteristic ($\tau^{-1} = 320$ kHz, $\alpha = 0.48$). This O-plasma experiment demonstrates that the percolating conductivity from the H-plasma treatment can be switched off, however, the dielectric relaxation mechanisms remain.

5.2 Raman Spectroscopy

Structural characterisation of the samples are shown in the Raman data in Fig. 4, revealing that the predominant phase in the as received BN ceramic is hexagonal (1364 cm^{-1}), with almost no detectable cubic phase (1055 cm^{-1}).[32,36] After H-plasma treatment, there is minimal change in the spectra with a similar result for the subsequent O-plasma treated sample. Curiously, a very small band is apparent at approximately 1580 cm^{-1} which is attributed to the G-Band of sp^2 carbon. This is most likely associated with the formation of trace carbon contaminants that have been incorporated into the ceramics from etching of the sample holder. Similarly, for the H_2 and vacuum annealed samples, the h-BN peak is apparent with a very small G-Band. However, the origin of this band is most likely associated

with contaminants from the graphite crucible during annealing. While carbon contaminated crucibles cannot be avoided, this band is incredibly small in comparison to the h-BN peak and only implies a very small concentration of carbon contamination. This is an interesting result and demonstrates that the increase in dielectric properties is less likely to be due to an increase in sp^2 carbon contamination since both the plasma and annealed samples show this band, even though sp^2 carbon is known to increase the complex permittivity of various materials.[26,37] However, Raman spectroscopy is not effective for the quantification of surface carbon features. Microscope images are given only for visual reference in Fig. 4 and show that there was minimal visual differences between the as received and the annealed sample; similar images were obtained for the wet and vacuum annealed samples. The plasma treated sample, however, showed significant discolouration.

5.3 X-Ray Photoelectron Spectroscopy

Quantification of the surface is measured using XPS, shown in Fig. 6. The untreated h-BN shows four distinct regions in the survey spectra, located at ca. 191, 285, 398 and 534 eV, attributed to the core B1s, C1s, N1s and O1s spectra respectively. Weak corresponding KLL spectra was also found at higher binding energies. The B1s spectra is ascribed to B-N bonding (190.6 eV), while the higher binding energy peaks (191.2 eV and 193.6 eV) with much lower intensity indicate concentrations of boric oxides such as B_2O_3 which are likely introduced by the binder.[38–40] The O1s spectra also shows these oxides associated with O=B (534) and O-B bonding (532.5 eV). The N1s spectra resolves two peaks associated with predominantly N-B bonding (398.2 eV) and some N-C bonding (398.8 eV). Finally, the C1s spectra shows C-C bonding (284.8 eV) and some C-O bonds (285.8 eV), attributed to surface adventitious carbon and contamination.[36,41] Note that the C=C peak at lower binding energies was not detected, implying that the marginal sp^2 carbon contributions observed in Raman is deeper than the XPS probing depth. Atomic percentages are given in Fig. 5, calculated by integrating the the background subtracted spectra and correcting for the

elemental sensitivity values, whereby a B:N atomic ratio of approximately 1.32:1 was found. The higher boron content is due to the boric oxides on the surface, as is corroborated by a high oxygen ratio. Additionally, the surface adventitious carbon contamination is significant at 14%.

After H-plasma treatment, the dominant 190.6 eV peak in the B1s spectra remains in all samples while the 193.6 eV peak became undetectable and the 534 eV peak in the O1s spectra has diminished (ca. 2%) and shifted to a lower binding energy of ca. 532.5 eV. This result has been reported in other works and is ascribed to a decreasing concentration of B_2O_3.[38] This implies that the trace binder surface components are etched in the H-plasma. The B-N peaks in the B1s and N1s spectra have increased in intensity and yield a B:N ratio of 1.07:1, indicative of a much cleaner h-BN surface. The C1s spectra has also decreased between the as received and the H-plasma treated (ca. 11%). After annealing in H_2, the samples are similar to the H-plasma treated sample although the O1s decrease is less dramatic (ca. 3 to 5%), and the surface carbon contamination is much lower (ca. 6 to 8%). After O-plasma treatment of the H-plasma treated sample, the BN ratio is similar at 1.1:1 although most notably the O1s spectra features a large O-B bonding peak, indicative of oxygen termination. The surface oxygen content increases to 10%, giving evidence towards removing the previous surface hydrogen with oxygen termination. Additionally, in the C1s spectra, another peak emerges which is associated with C=O bonding (288.9 eV).

6 Discussion

The complex permittivity data of the untreated h-BN results are similar to the calculated values reported by several authors.[5,7,35] For h-BN, the 2D structure inherently implies anisotropy, to which the anticipated bulk complex permittivity in-plane ($\varepsilon_{r,\parallel}$) is dissimilar to the out-of-plane value ($\varepsilon_{r,\perp}$); calculations demonstrate that electronic polarisation predominantly contributes with $\varepsilon_{r,\parallel} > \varepsilon_{r,\perp}$.[35] Even though the field orientations vary amongst

PPC, BCP and MCP, anisotropy is not measured implying that the macroscopic dielectric properties of hot-pressed h-BN ceramics is isotropic.

The most pertinent finds in this study are (i) the dielectric properties of h-BN when annealed in H_2 at ~ 800 °C are minimally changed, (ii) when exposed to atomic H, a huge amplification occurs with an associated relaxation in the megahertz range in addition to (iii) a long range conduction mechanism and finally (iv) the disappearance of the long range conduction after a short oxygen plasma exposure.

In the case of (i), the temperature stability of h-BN has been demonstrated and that tube furnace type CVD methods to deposit graphene are seemingly least likely to damage the insulating properties of the h-BN. The peculiar result of (ii) and (iii) demonstrates that atomic H leads to an enhanced complex permittivity including a DC conductivity. A diagram of the following explanation is given in Fig. 7. The DC conductivity is due to percolating pathways on the surface and in the bulk. The enhanced complex permittivity and HN relaxation likely stems from a form of Maxwell-Sillars-Wagner type polarisation of an insulating host medium with small conducting regions and pathways.[42] In an electric field, the charges migrate along these pathways and are impeded by the insulating boundaries, resulting in charge build-up and an amplified capacitance effect. At shorter timescales, or higher frequencies, these charges never polarise resulting in relaxation at a characteristic time ($\tau^{-1} = 150$ MHz in Fig. 2). Additionally, after the short O-plasma exposure, most of the surface conducting regions are removed including direct connection to the percolating ones. This is the reason why the DC conductivity disappears and instead a lower frequency relaxation is observed since now the charges are impeded by the less conductive oxygen terminated surface ($\tau^{-1} = 320$ kHz in Fig. 2).

For the plasma treated h-BN, however, regions of some conducting phase must exist. There are a number of possibilities for this, where the less likely causes are explained first. The first is electronic modification due to B or N vacancy formation as the BN is etched in the hydrogen plasma. There are numerous density functional theory (DFT) studies on

the vacancy formation in h-BN sheets which all show that the electronic properties of h-BN are altered.[43–45] Huang and Lee demonstrated using a DFT model that introducing vacancies at both B and N sites creates several mid-gap states, although seemingly deep at several eV from the valence band minimum.[44] This implies that vacancy formation is not the principal cause of the increased room temperature conductivity observed in the present study. A second possibility is due to band gap narrowing of h-BN using an RF O-plasma. In this notable study, the plasma is used to create nitrogen vacancies to substitute in oxygen which results in a lower resistivity to pristine h-BN.[46] In the present study, after H-plasma treatment, when the sample is brought to atmosphere, surface oxygen could be incorporated, however, further exposing this sample to O-plasma increases the oxygen and removes the conductivity. A third possibility is that the h-BN is affected by the diffusion and intercalation of H_2 into the bulk at elevated temperatures. Since H_2 annealing only resulted in a small decrease in the overall dielectric constant and a very small increase in the low frequency loss this is likely not responsible. Also, attempts to encourage H_2 uptake through wetting gave minimal change, even though the binder is very hygroscopic. A fourth possibility is due to the low melting point of the boric acid binder which may dissociate at higher temperatures causing the electrical properties to change. Annealing in vacuum gave similar results to the H_2 annealed, implying that the enhancement is not due to any temperature related phase changes associated with the binder. Finally, one of the most obvious possibilities is that sp^2 carbon contamination from the sample holder has become incorporated into the h-BN. This case is not as likely because similar sp^2 carbon concentrations were found in both the plasma treated and annealed samples. At first the C1s results seemingly contradict the Raman data, however, it is noted that the predominant binding energy peak is that of C-C character and not C=C. Hence, the first ca. 10 nm of the surface (as probed by XPS) is covered with surface adventitious carbon layer after exposure to air and at greater depths (as probed by Raman), formation of sp^2 carbon which has diffused between the h-BN layers is found. From a macroscopic dielectric perspective, the sp^2 carbon observed at further depths has made

little difference to the measured complex permittivity.

With no evidence of increasing oxygen or carbon in the H-plasma treated sample but the subsequent O-plasma treated surface decreases the conductivity leads to the most likely cause to being full or partial surface hydrogenation. The exposure of the h-BN ceramic to atomic hydrogen results in hydrogen termination of surface and bulk regions of h-BN which are separated by the binder. One theory is that hydrogen termination is known to produce a negative electron affinity (NEA),[47] which in turn promotes surface conductivity,[48] similar to that in hydrogen terminated diamond.[49,50] Although, full hydrogenation of the h-BN sheets is likely not responsible for the enhanced conduction losses as it is also known that while this does indeed decrease the wide band gap, it does not create significant mid gap states to allow room temperature conductivity.[45] It was, however, calculated that metallic conduction is possible with semi-hydrogenated BN layers, whereby only the B atoms are bonded to hydrogen.[45] This form of semi-hydrogenation, as opposed to full hydrogenation and just hydrogen bonding to N atoms, is seemingly stable and gives rise to a metallic BN character, in addition to a distorted and buckled lattice structure.

There are not many techniques which can confirm the hydrogenation directly; XPS is not sensitive to hydrogen and so one would not expect a significant perturbation or additional peaks in the B1s or N1s spectra. For the B1s spectra, the escape depth of a photoelectron is approximately 32 Å and therefore the total information depth for the obtained spectra is around 3 times this value (ca. 10 nm). Since the surface component of this (B-H bond of around 1.2 Å[45,51]) is so small in comparison to the probing depth no change may be measured. Additionally, since only select areas of the surface are semi-hydrogenated, this further reduces the possibility of measuring. However, the sharp decrease in all other surface elements (carbon and oxygen) after exposure to atomic hydrogen still provides inference towards hydrogen termination. Thus, this is the most plausible explanation behind the increased dielectric properties of the h-BN in that the hydrogen plasma exposure results in locally high dielectric loss, or electrically conducting, islands of semi-hydrogenated h-BN, as

is shown in the representation given in Fig. 8. This also explains why the H_2 annealed h-BN yielded minimal change in ε_r, as molecular hydrogen does not hydrogenate the h-BN layer, as this is only achieved with the high energy density plasma. Further precedence to this is that several DFT studies demonstrate that H_2 bonding to BN is not stable.[45]

This result demonstrates that microwave plasma CVD of any material onto a h-BN dielectric substrate is ill-advised. As a demonstration, a similar dielectric amplification result was obtained when several microns of CVD diamond was deposited on the h-BN sample. Using the same conditions except with an additional 5% CH_4 in the gas phase, the amplification was larger ($\varepsilon_s \approx 45$, $\varepsilon_\infty \approx 8$, $\tau^{-1} \approx 770$ MHz) in addition to a finite long range conductivity of 8 mS/m (see Supporting Information, Fig. S1). The larger conductivity reported here is due to the additional contributions from the non-diamond carbon impurities and potential leeching of boron into the diamond layer, however, these mechanisms are out of scope of this study. Moving forward with other new and exciting applications of h-BN, however, h-BN is a promising hydrogen storage material to which the detection of changes in dielectric property may infer the concentration of adsorbed atomic hydrogen on B sites. This of course can be easily achieved with the above non-destructive and non-contact methods (MCP in particular).[12,52,53]

7 Conclusion

In conclusion, it is demonstrated that the complex permittivity of h-BN has a low dielectric constant and an immeasurably low dielectric loss across the kilohertz to gigahertz frequency range. A dramatic increase in complex permittivity is observed after exposure to atomic hydrogen, resulting in dispersive features. The importance of this work draws attention to the fact that while popular microwave plasma CVD methods are capable of producing graphene on Cu substrates, the desire to move away from metal catalysts and use similar techniques for h-BN must be approached with caution. Annealing studies here demonstrate that adopting

tube furnace CVD techniques are a lower risk approach to retaining low dielectric constant h-BN when directly depositing graphene. For other applications including sensing and other electronic applications, it has been demonstrated that the conductivity of h-BN can be tuned through hydrogenation in a microwave plasma, although, it is not only the surface that is modified but the bulk also owing to atomic H diffusion.

Acknowledgement

JAC acknowledges financial support of the Engineering and Physical Sciences Research Council under the program Grant GaN-DaME (EP/P00945X/1). SM and OAW acknowledge financial support of the European Research Council (ERC) Consolidator Grant SUPERNEMS, Project ID: 647471. XP Spectra were recorded at the Cardiff hub of the ESPRC National Facility for X-Ray Photoelectron Spectroscopy ('HarwellXPS'), operated by Cardiff University and UCL under contract number PR16195. JAC would also like to thank Greg Shaw for his technical support.

Supporting Information Available

Supporting Information Available: Additional dielectric spectroscopy data of the CVD grown diamond films on h-BN ceramics.

References

(1) Šiškins, M.; Mullan, C.; Son, S.-K.; Yin, J.; Watanabe, K.; Taniguchi, T.; Ghazaryan, D.; Novoselov, K. S.; Mishchenko, A. High-temperature electronic devices enabled by hBN-encapsulated graphene. *Applied Physics Letters* **2019**, *114*, 123104.

(2) Barnard, H. R.; Zossimova, E.; Mahlmeister, N. H.; Lawton, L. M.; Luxmoore, I. J.;

Nash, G. R. Boron nitride encapsulated graphene infrared emitters. *Applied Physics Letters* **2016**, *108*, 131110.

(3) Dauber, J.; Sagade, A. A.; Oellers, M.; Watanabe, K.; Taniguchi, T.; Neumaier, D.; Stampfer, C. Ultra-sensitive Hall sensors based on graphene encapsulated in hexagonal boron nitride. *Applied Physics Letters* **2015**, *106*, 193501.

(4) Wang, J.; Ma, F.; Sun, M. Graphene, hexagonal boron nitride, and their heterostructures: properties and applications. *RSC Advances* **2017**, *7*, 16801–16822.

(5) Kumar, P.; Chauhan, Y. S.; Agarwal, A.; Bhowmick, S. Thickness and Stacking Dependent Polarizability and Dielectric Constant of Graphene-Hexagonal Boron Nitride Composite Stacks. *Journal of Physical Chemistry C* **2016**, *120*, 17620–17626.

(6) Ji, Y.; Pan, C.; Zhang, M.; Long, S.; Lian, X.; Miao, F.; Hui, F.; Shi, Y.; Larcher, L.; Wu, E.; Lanza, M. Boron nitride as two dimensional dielectric: Reliability and dielectric breakdown. *Applied Physics Letters* **2016**, *108*, 012905.

(7) Kim, K. K.; Hsu, A.; Jia, X.; Kim, S. M.; Shi, Y.; Dresselhaus, M.; Palacios, T.; Kong, J. Synthesis and characterization of hexagonal boron nitride film as a dielectric layer for graphene devices. *ACS Nano* **2012**, *6*, 8583–8590.

(8) Chen, X.; Cheng, Y.; Wu, K.; Xie, X. Dielectric spectroscopy analysis of the h-BN ceramic. *Journal of Physics D: Applied Physics* **2007**, *40*, 6034–6038.

(9) Nose, K.; Oba, H.; Yoshida, T. Electric conductivity of boron nitride thin films enhanced by in situ doping of zinc. *Applied Physics Letters* **2006**, *89*, 112124.

(10) Pang, H.; Pang, W.; Zhang, B.; Ren, N. Excellent microwave absorption properties of the h-BN–GO–Fe 3 O 4 ternary composite. *Journal of Materials Chemistry C* **2018**, *6*, 11722–11730.

(11) Zhou, W.; Xiao, P.; Li, Y. Preparation and study on microwave absorbing materials of boron nitride coated pyrolytic carbon particles. *Applied Surface Science* **2012**, *258*, 8455–8459.

(12) Merlo, A.; Mokkapati, V. R. S. S.; Pandit, S.; Mijakovic, I. Boron nitride nanomaterials: biocompatibility and bio-applications. *Biomaterials Science* **2018**, *6*, 2298–2311.

(13) Hoang, D. Q.; Korneychuk, S.; Sankaran, K. J.; Pobedinskas, P.; Drijkoningen, S.; Turner, S.; Van Bael, M. K.; Verbeeck, J.; Nicley, S. S.; Haenen, K. Direct nucleation of hexagonal boron nitride on diamond: Crystalline properties of hBN nanowalls. *Acta Materialia* **2017**, *127*, 17–24.

(14) Woehrl, N.; Ochedowski, O.; Gottlieb, S.; Shibasaki, K.; Schulz, S. Plasma-enhanced chemical vapor deposition of graphene on copper substrates. *AIP Advances* **2014**, *4*, 047128.

(15) Fang, L.; Yuan, W.; Wang, B.; Xiong, Y. Growth of graphene on Cu foils by microwave plasma chemical vapor deposition: The effect of in-situ hydrogen plasma post-treatment. *Applied Surface Science* **2016**, *383*, 28–32.

(16) Kostoglou, N.; Polychronopoulou, K.; Rebholz, C. Thermal and chemical stability of hexagonal boron nitride (h-BN) nanoplatelets. *Vacuum* **2015**, *112*, 42–45.

(17) Konyashin, I.; Aldinger, F.; Babaev, V.; Khvostov, V.; Guseva, M.; Bregadze, A.; Baumgärtner, K.-M.; Räuchle, E. The mechanism of cubic boron nitride deposition in hydrogen plasmas. *Thin Solid Films* **1999**, *355-356*, 96–104.

(18) Khvostov, V.; Konyashin, I.; Shouleshov, E.; Babaev, V.; Guseva, M. Surface modification of boron nitride in hydrogen plasma. *Applied Surface Science* **2000**, *157*, 178–184.

(19) He, L.; Wang, H.; Chen, L.; Wang, X.; Xie, H.; Jiang, C.; Li, C.; Elibol, K.; Meyer, J.; Watanabe, K.; Taniguchi, T.; Wu, Z.; Wang, W.; Ni, Z.; Miao, X.; Zhang, C.; Zhang, D.;

Wang, H.; Xie, X. Isolating hydrogen in hexagonal boron nitride bubbles by a plasma treatment. *Nature Communications* **2019**, *10*, 1–9.

(20) Son, M.; Lim, H.; Hong, M.; Choi, H. C. Direct growth of graphene pad on exfoliated hexagonal boron nitride surface. *Nanoscale* **2011**, *3*, 3089.

(21) Kim, S. M.; Hsu, A.; Araujo, P. T.; Lee, Y.-H.; Palacios, T.; Dresselhaus, M.; Idrobo, J.-C.; Kim, K. K.; Kong, J. Synthesis of Patched or Stacked Graphene and hBN Flakes: A Route to Hybrid Structure Discovery. *Nano Letters* **2013**, *13*, 933–941.

(22) Arjmandi-Tash, H.; Kalita, D.; Han, Z.; Othmen, R.; Nayak, G.; Berne, C.; Landers, J.; Watanabe, K.; Taniguchi, T.; Marty, L.; Coraux, J.; Bendiab, N.; Bouchiat, V. Large scale graphene/h-BN heterostructures obtained by direct CVD growth of graphene using high-yield proximity-catalytic process. *Journal of Physics: Materials* **2018**, *1*, 015003.

(23) Shi, G.; Hanlumyuang, Y.; Liu, Z.; Gong, Y.; Gao, W.; Li, B.; Kono, J.; Lou, J.; Vajtai, R.; Sharma, P.; Ajayan, P. M. Boron Nitride–Graphene Nanocapacitor and the Origins of Anomalous Size-Dependent Increase of Capacitance. *Nano Letters* **2014**, *14*, 1739–1744.

(24) Madelung, O.; Rossler, U.; Schulz, M. In *Group IV Elements, IV-IV and III-V Compounds. Part a - Lattice Properties*; Madelung, O., Rössler, U., Schulz, M., Eds.; Landolt-Börnstein - Group III Condensed Matter 0; Springer-Verlag: Berlin/Heidelberg, 2001; Vol. a; pp 1–5.

(25) Cuenca, J. A.; Thomas, E. L. H.; Mandal, S.; Williams, O.; Porch, A. Investigating the broadband microwave absorption of nanodiamond impurities. *IEEE Transactions on Microwave Theory and Techniques* **2015**, *63*, 4110–4118.

(26) Cuenca, J. A.; Sankaran, K. J.; Pobedinskas, P.; Panda, K.; Lin, I.-N.; Porch, A.;

Haenen, K.; Williams, O. A. Microwave cavity perturbation of nitrogen doped nanocrystalline diamond films. *Carbon* **2019**, *145*, 740–750.

(27) Ding, M.; Liu, Y.; Lu, X.; Li, Y.; Tang, W. Boron doped diamond films: A microwave attenuation material with high thermal conductivity. *Applied Physics Letters* **2019**, *114*, 162901.

(28) Eichelbaum, M.; Stößer, R.; Karpov, A.; Dobner, C.-K.; Rosowski, F.; Trunschke, A.; Schlögl, R. The microwave cavity perturbation technique for contact-free and in situ electrical conductivity measurements in catalysis and materials science. *Phys. Chem. Chem. Phys.* **2012**, *14*, 1302–1312.

(29) Krupka, J.; Breeze, J.; Centeno, A.; Alford, N.; Claussen, T.; Jensen, L. Measurements of permittivity, dielectric loss tangent, and resistivity of float-zone silicon at microwave frequencies. *IEEE Transactions on Microwave Theory and Techniques* **2006**, *54*, 3995–4000.

(30) Liu, C.; Xiao, X.; Wang, J.; Shi, B.; Adiga, V. P.; Carpick, R. W.; Carlisle, J. A.; Auciello, O. Dielectric properties of hydrogen-incorporated chemical vapor deposited diamond thin films. *Journal of Applied Physics* **2007**, *102*, 074115.

(31) Cuenca, J. A.; Thomas, E. L. H.; Mandal, S.; Williams, O. A.; Porch, A. Microwave determination of sp2 carbon fraction in nanodiamond powders. *Carbon* **2015**, *81*, 174–178.

(32) Mandal, S.; Bland, H. A.; Cuenca, J. A.; Snowball, M.; Williams, O. A. Superconducting boron doped nanocrystalline diamond on boron nitride ceramics. *Nanoscale* **2019**, *11*, 10266–10272.

(33) Colosi, C.; Costantini, M.; Barbetta, A.; Cametti, C.; Dentini, M. Anomalous Debye-like dielectric relaxation of water in micro-sized confined polymeric systems. *Physical Chemistry Chemical Physics* **2013**, *15*, 20153.

(34) Porch, A.; Slocombe, D.; Beutler, J.; Edwards, P.; Aldawsari, A.; Xiao, T.; Kuznetsov, V.; Almegren, H.; Aldrees, S.; Almaqati, N. Microwave treatment in oil refining. *Applied Petrochemical Research* **2012**, *2*, 37–44.

(35) Laturia, A.; Van de Put, M. L.; Vandenberghe, W. G. Dielectric properties of hexagonal boron nitride and transition metal dichalcogenides: from monolayer to bulk. *npj 2D Materials and Applications* **2018**, *2*, 6.

(36) Fang, H.; Zhang, X.; Zhao, Y.; Bai, S.-L. Dense graphene foam and hexagonal boron nitride filled PDMS composites with high thermal conductivity and breakdown strength. *Composites Science and Technology* **2017**, *152*, 243–253.

(37) Lv, H.; Guo, Y.; Zhao, Y.; Zhang, H.; Zhang, B.; Ji, G.; Xu, Z. J. Achieving tunable electromagnetic absorber via graphene/carbon sphere composites. *Carbon* **2016**, *110*, 130–137.

(38) Wang, Y.; Trenary, M. Surface chemistry of boron oxidation. 2. The reactions of boron oxides B2O2 and B2O3 with boron films grown on tantalum(110). *Chemistry of Materials* **1993**, *5*, 199–205.

(39) Li, Y.; Yang, M.; Xu, B.; Sun, Q.; Zhang, W.; Zhang, Y.; Meng, F. Synthesis, structure and antioxidant performance of boron nitride (hexagonal) layers coating on carbon nanotubes (multi-walled). *Applied Surface Science* **2018**, *450*, 284–291.

(40) Zhong, B.; Cheng, Y.; Wang, M.; Bai, Y.; Huang, X.; Yu, Y.; Wang, H.; Wen, G. Three dimensional hexagonal boron nitride nanosheet/carbon nanotube composites with light weight and enhanced microwave absorption performance. *Composites Part A: Applied Science and Manufacturing* **2018**, *112*, 515–524.

(41) Mishra, N.; Miseikis, V.; Convertino, D.; Gemmi, M.; Piazza, V.; Coletti, C. Rapid and catalyst-free van der Waals epitaxy of graphene on hexagonal boron nitride. *Carbon* **2016**, *96*, 497–502.

(42) Sihvola, A. In *Electromagnetic Mixing Formulas and Applications*, illustrate ed.; Sihvola, A. H., Ed.; IET: The Institution of Engineering and Technology, Michael Faraday House, Six Hills Way, Stevenage SG1 2AY, UK, 1999; p 81.

(43) Späth, F.; Gebhardt, J.; Düll, F.; Bauer, U.; Bachmann, P.; Gleichweit, C.; Görling, A.; Steinrück, H.-P.; Papp, C. Hydrogenation and hydrogen intercalation of hexagonal boron nitride on Ni(1 1 1): reactivity and electronic structure. *2D Materials* **2017**, *4*, 035026.

(44) Huang, B.; Lee, H. Defect and impurity properties of hexagonal boron nitride: A first-principles calculation. *Physical Review B* **2012**, *86*, 245406.

(45) Wang, Y. Electronic properties of two-dimensional hydrogenated and semihydrogenated hexagonal boron nitride sheets. *physica status solidi (RRL) - Rapid Research Letters* **2010**, *4*, 34–36.

(46) Sevak Singh, R.; Yingjie Tay, R.; Leong Chow, W.; Hon Tsang, S.; Mallick, G.; Tong Teo, E. H. Band gap effects of hexagonal boron nitride using oxygen plasma. *Applied Physics Letters* **2014**, *104*, 163101.

(47) Powers, M. J.; Benjamin, M. C.; Porter, L. M.; Nemanich, R. J.; Davis, R. F.; Cuomo, J. J.; Doll, G. L.; Harris, S. J. Observation of a negative electron affinity for boron nitride. *Applied Physics Letters* **1995**, *67*, 3912–3914.

(48) He, B.; Ng, T.-W.; Lo, M.-F.; Lee, C.-S.; Zhang, W. Surface Transfer Doping of Cubic Boron Nitride Films by MoO 3 and Tetrafluoro-tetracyanoquinodimethane (F4-TCNQ). *ACS Applied Materials & Interfaces* **2015**, *7*, 9851–9857.

(49) Williams, O. A.; Jackman, R. B. Surface conductivity on hydrogen terminated diamond. *Semiconductor Science and Technology* **2003**, *18*, S34–S40.

(50) Landstrass, M. I.; Ravi, K. V. Hydrogen passivation of electrically active defects in diamond. *Applied Physics Letters* **1989**, *55*, 1391–1393.

(51) Ponce-Pérez, R.; Cocoletzi, G. H. Hydrogenated boron nitride monolayer functionalization: A density functional theory study. *Computational and Theoretical Chemistry* **2017**, *1111*, 33–39.

(52) Lale, A.; Bernard, S.; Demirci, U. B. Boron Nitride for Hydrogen Storage. *ChemPlusChem* **2018**, *83*, 893–903.

(53) Hartley, J.; Porch, A.; Jones, M. A non-invasive microwave method for assessing solid-state ammonia storage. *Sensors and Actuators B: Chemical* **2015**, *210*, 726–730.

8 Figures and Tables

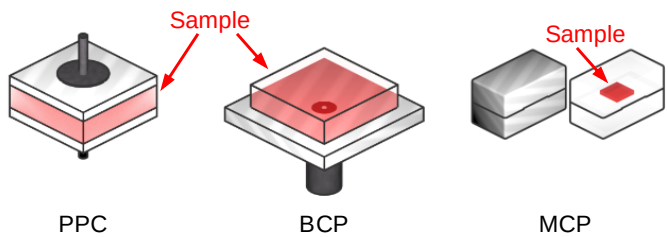

Figure 1: Graphical representation of the methods used in this study

Table 1: Tabulated dielectric constant of PTFE and h-BN samples

Method*	PPC	BCP	MCP (Al Cavity)			MCP (WG14 Cavity)			
f (GHz)	$10^{-6 \text{ to } -3}$	$10^{-2 \text{ to } 1}$	2.5	4.6	5.5	4.5	5.6	7.4	9.6
PTFE	2.05	2.05	2.05	2.05	2.05	2.05	2.05	2.05	2.05
h-BN	4.3	4.2	4.320	4.298	4.275	4.309	4.287	4.221	4.143
h-BN (HP)	20	20 to 4.2	4.726	4.636	4.309	4.691	4.482	4.282	4.101
h-BN (HP & OP)	20 to 14	20 to 4.2	4.428	4.533	3.990	4.533	4.424	4.071	3.892
h-BN (H_2 Anneal, Dry)	3.9	3.6	3.796	3.991	3.754	4.146	4.060	3.969	3.669
h-BN (H_2 Anneal, Wet)	4.3	4.2	3.948	4.135	3.972	4.240	4.158	4.087	3.835
h-BN (Vac. Anneal, Dry)	3.7	4.5	3.807	4.018	3.855	4.021	3.951	3.940	3.640
h-BN (Vac. Anneal, Wet)	3.8	4.2	4.016	4.254	3.931	4.056	3.949	3.922	3.725

*Maximum standard deviation of 6 samples of approximately ± 0.1, ± 0.2 and $\pm 6 \times 10^{-3}$ for PPC, BCP and MCP, respectively.

Table 2: Tabulated dielectric of loss PTFE and h-BN samples

Method*	PPC	BCP	MCP (Al Cavity)			MCP (WG14 Cavity)			
f (GHz)	$10^{-6 \text{ to } -3}$	$10^{-2 \text{ to } 1}$	2.5	4.6	5.5	4.5	5.6	7.4	9.6
PTFE	0	0	0.002	0	0	0.006	0	0.03	0.2
h-BN	0	0	0.006	0.004	0.004	0.01	0	0.06	0.4
h-BN (HP)	$0.00032/\omega\varepsilon_0$	6.4 to 0	1.48	0.97	0.76	3.97	0.77	0.55	0.38
h-BN (HP & OP)	0 to 5	5 to 0	0.54	0.38	0.29	0.38	0.35	0.23	0.05
h-BN (Vac. Anneal, Dry)	0.5 to 0	0	0	0	0	0.009	0	0.07	0.04
h-BN (Vac. Anneal, Wet)	0.2 to 0	0	0	0.004	0.002	0.01	0	0.02	0
h-BN (H_2 Anneal, Dry)	0.4 to 0	0	0	0	0	0.01	0	0.06	0
h-BN (H_2 Anneal, Wet)	0.2 to 0	0	0	0.003	0.002	0.02	0	0.05	0

*Maximum standard deviation of 6 samples of approximately ± 0.1, ± 0.2 and $\pm 6 \times 10^{-3}$ for PPC, BCP and MCP, respectively.

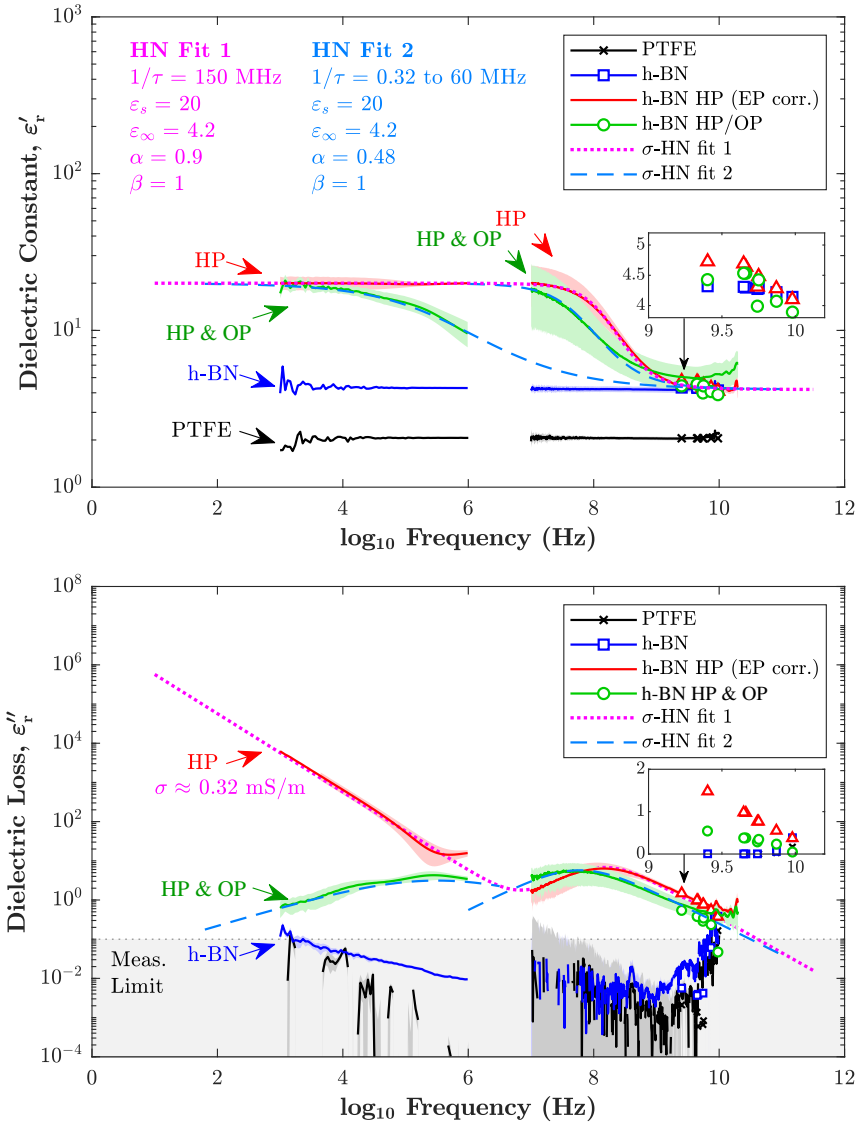

Figure 2: Complex permittivity of PTFE, h-BN, H-plasma treated (HP) and subsequent O-plasma treated (OP) samples obtained using PPC, BCP and MCP with the σ-HN model from (2) and (3). EP correction provides an estimate of free charge conductivity. Shaded regions show the uncertainty: the standard deviation of 6 sample measurements and instrumental limitation.

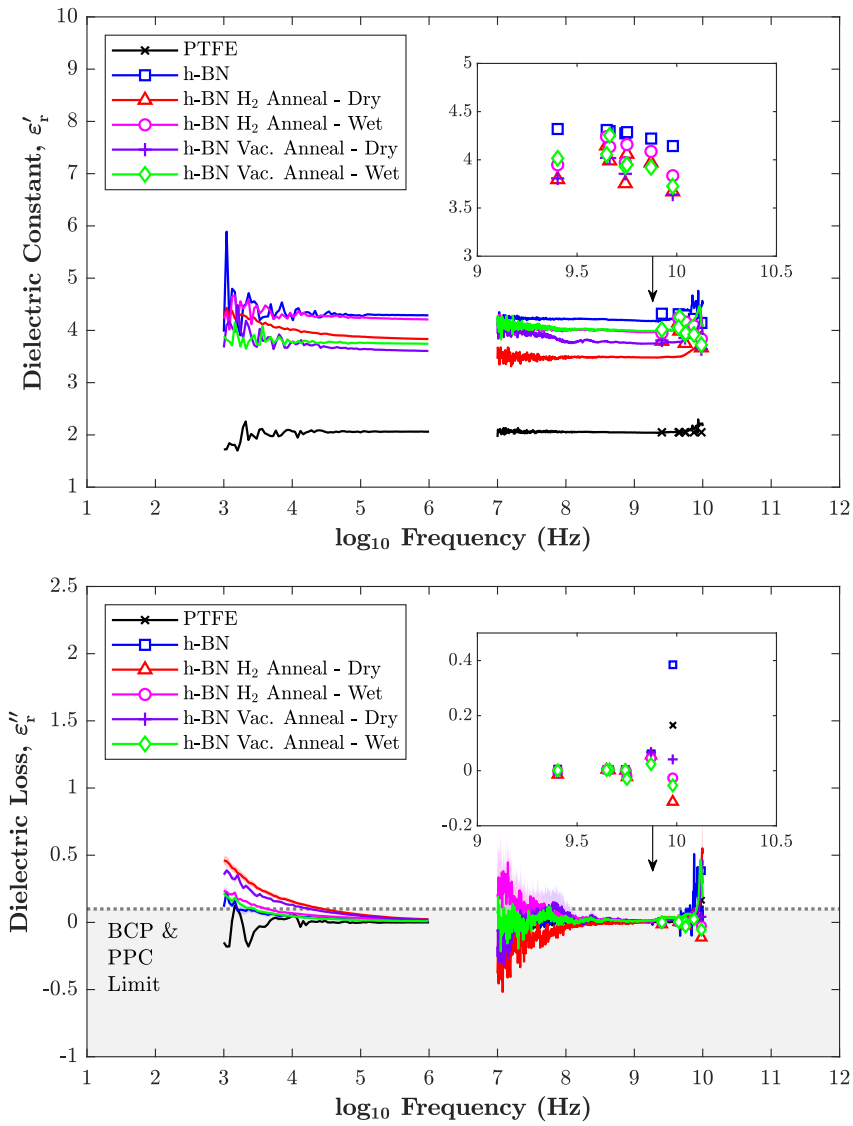

Figure 3: Complex permittivity of PTFE standard, h-BN and annealed h-BN samples obtained using PPC, BCP and MCP. The shaded regions mark the uncertainty: the standard error of 6 sample measurements and instrumental limitation.

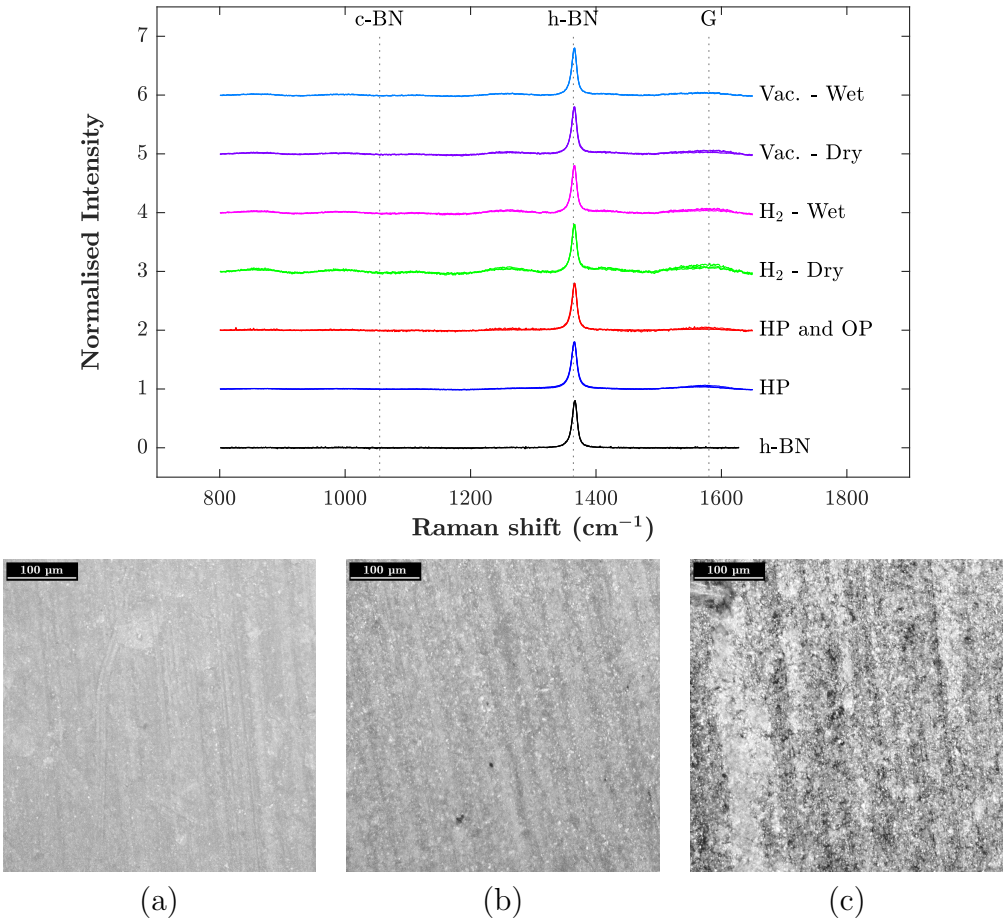

Figure 4: Raman Spectroscopy (top) and microscope images (bottom) of hydrogen treated h-BN samples. Data shows three spectra of each sample overlaid with all peaks normalised to the h-BN peak with background correction. No significant variations in composition are noticed although a small G-band is found in all treated samples. Microscope images (20× magnification) of (a) as received h-BN , (b) H_2 dry annealed and (c) H-Plasma treated samples are given only for visual reference of the surface roughening.

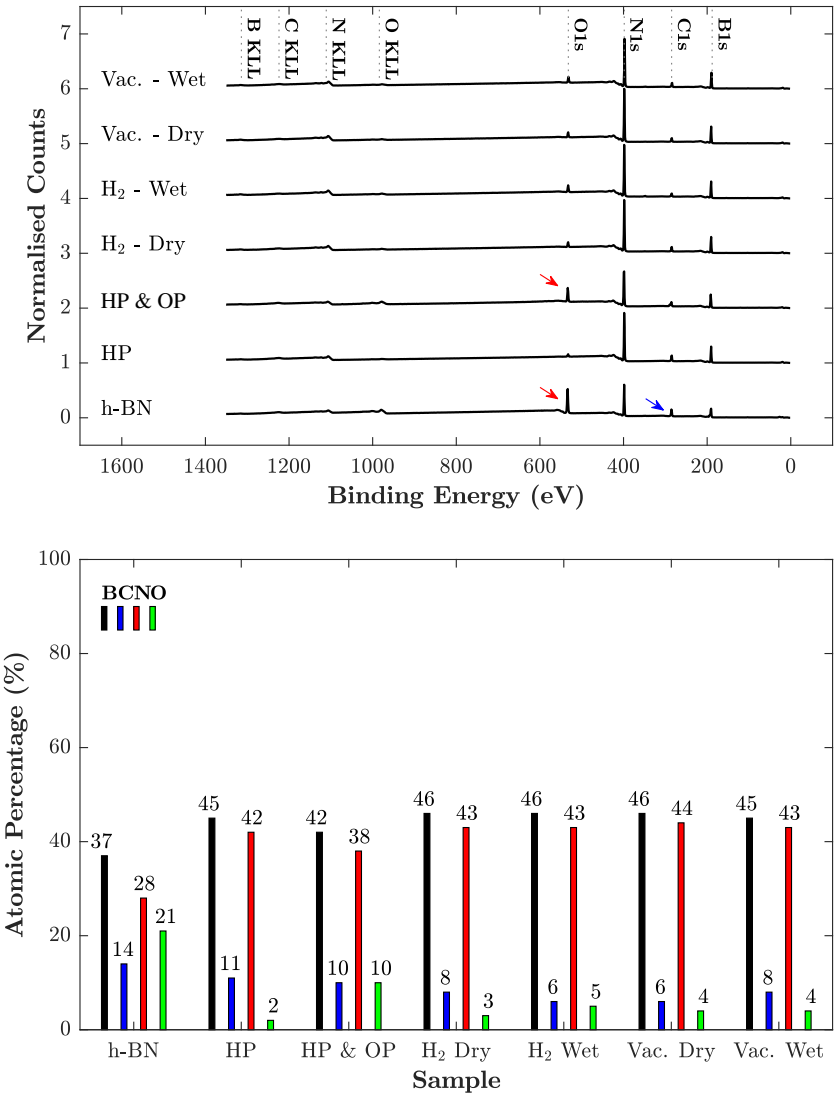

Figure 5: XPS survey (top) and atomic ratios of h-BN samples. Arrows in survey denote pertinent differences after treatment. Relative Sensitivity factors for B, C, N and O are given as 0.486, 1, 1.8 and 2.93, respectively.

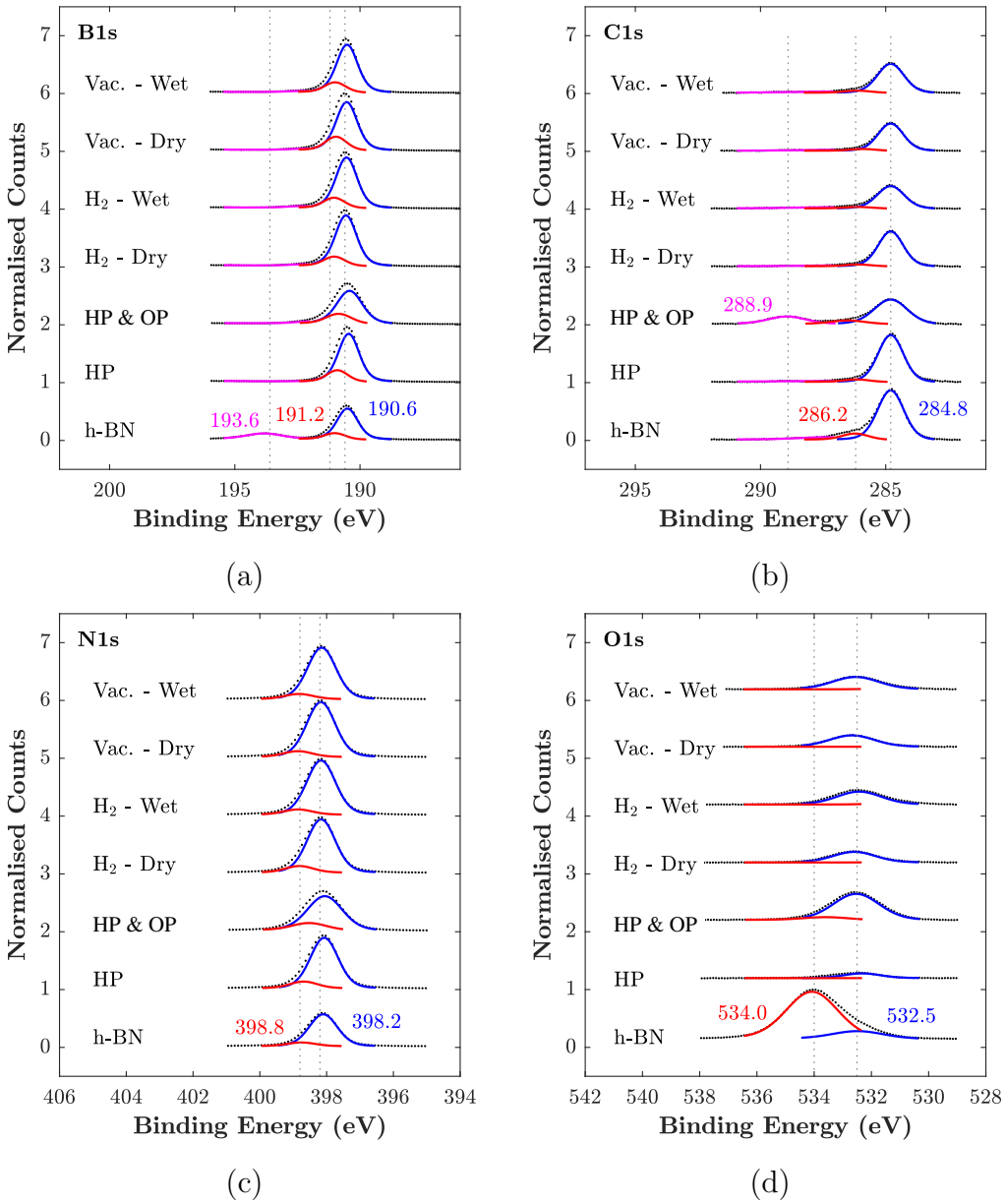

Figure 6: XPS data of h-BN samples all normalised to the largest N1s peak: (a) B1s (b) C1s, (c) N1s and (d) O1s.

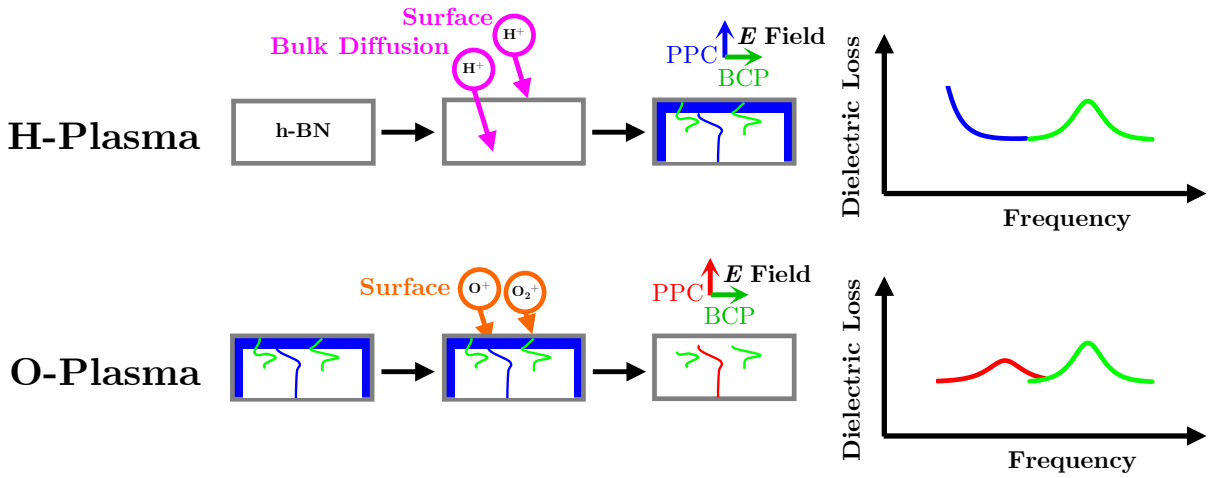

Figure 7: Representative diagram of conducting pathways created by the H-plasma (top) and truncation of pathways by removing surface termination with O-plasma (bottom). The atomic H reacts with the surface and the bulk of the h-BN to create various electrically conducting pathways which are measured by PPC and BCP, blue and green traces, respectively. The oxygen plasma removes most of the surface conductivity, leaving bulk long and short pathways, as measured by PPC and BCP, red and green traces, respectively.

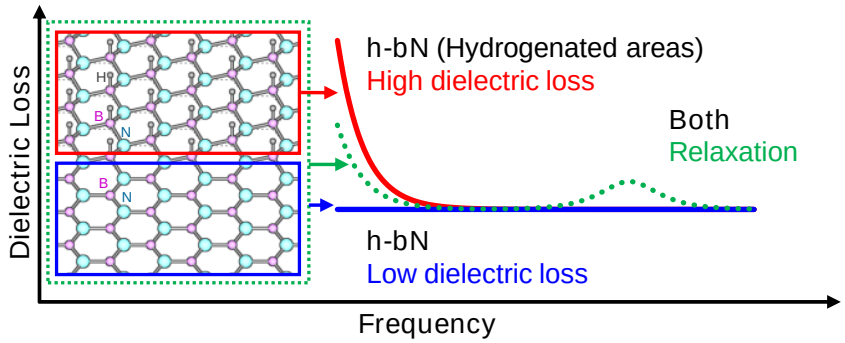

Figure 8: Representative model of low and high dielectric loss regions from as received and hydrogenated h-BN, respectively. Long range conduction results from percolating hydrogenated h-BN pathways whereas finite regions result in Debye type relaxation.

Graphical TOC Entry